Research Square

Preprints are preliminary reports that have not undergone peer review.
They should not be considered conclusive, used to inform clinical practice,
or referenced by the media as validated information.

Box-Behnken Optimization of Turning Parameters for Minimal Surface Roughness and Corrosion Integrity of SS316L

Zohan Ardiansyah
Universitas Negeri Surabaya
Hanna Zakiyya
Universitas Negeri Surabaya
Slamet Prasetyo Utomo
Universitas Negeri Surabaya
Diah N. Syafitri
Universitas Negeri Surabaya
Agus Nugroho
National Reseach and Innovation Agency (BRIN), South Tangerang
Mochamad Arif Irfa'i
arifirfai@unesa.ac.id

Universitas Negeri Surabaya

Research Article

Keywords: Stainless steel 316L, surface roughness, response surface methodology, turning, orthopedic implant

Posted Date: November 20th, 2026

DOI: https://doi.org/10.21203/rs.3.rs-11559704/v1

License: This work is licensed under a Creative Commons Attribution 4.0 International License.
Read Full License

Additional Declarations: No competing interests reported.

Box-Behnken Optimization of Turning Parameters for Minimal Surface Roughness and Corrosion Integrity of SS316L

Statements and Declarations

No funding was received to prepare this article.

The authors have no conflict of interest to declare.

ABSTRACT

this study investigates the optimization of machining parameters for turning SS316L stainless steel, a material widely used for medical and orthopedic implants. Controlling surface roughness is critical for the material's performance in physiological environments. The researchers employed Response Surface Methodology (RSM) with a three-factor, three-level Box-Behnken Design consisting of 17 experimental runs to minimize the arithmetic mean roughness (R_a). The independent variables analyzed were spindle speed, feed rate, and depth of cut. The analysis revealed that only feed rate significantly impacts the surface roughness of the SS316L workpiece. The numerical optimization predicted a minimum R_a of 0.2327 μm using a feed rate of 0.063 mm/rev, a spindle speed of 1450 rpm, and a depth of cut of 0.08 mm. Experimental validation at these optimal conditions achieved an actual R_a of 0.244 μm, demonstrating a minor 4.7% deviation from the model's prediction. Furthermore, the optimized specimen was evaluated using Atomic Force Microscopy (AFM), which identified micro-grooves and localized topographical variations caused by built-up edges. Finally, potentiodynamic polarization testing in Simulated Body Fluid (SBF) determined a corrosion rate of 6.54×10^{-5} mm/year, providing a comprehensive assessment of the implant material's durability in a simulated body environment.

Keywords: Stainless steel 316L, surface roughness; response surface methodology; turning; orthopedic implant.

Introduction

Stainless steel 316L (SS316L) is widely used in biomedical applications, including orthopedic implants, owing to its adequate mechanical properties and corrosion resistance[1,2]. However, because bare SS316L is biologically inert, it is most frequently utilized as a load-bearing metallic substrate beneath functional bioactive coatings. Among these, hydroxyapatite (HAp) is the most prominent and widely applied, serving to enhance osteoblast proliferation, accelerate osseointegration, and establish direct chemical bonding with adjacent host bone tissue [3,4].

To maintain long-term clinical efficacy, the interfacial adhesion strength between the bioactive coating and the metallic substrate remains a critical limiting factor. Consequently, controlling surface roughness and topography is important to ensure coating integrity. Effective surface pre-treatment cleans the substrate, increases surface energy, and provides micro-mechanical interlocking sites that enhance bonding, reduce residual stress concentration, and prevent catastrophic coating delamination under in vivo physiological loads [2,5,6].

Previous studies have demonstrated that machining parameters influence the surface characteristics of SS316L. Szwajka et al. [6] reported that cutting speed and feed rate affect surface roughness and the characteristics of the near-surface layer of AISI 316L. Farooq et al. [7] optimized the turning parameters of additively manufactured SS316L by considering surface roughness and tool life, whereas Risco-Alfonso et al. [8] investigated cutting-condition optimization based on tool wear progression. These findings highlight the importance of machining parameter selection, although the surface characteristics and responses investigated depend on the objectives and process conditions of each study. Response Surface Methodology (RSM) can be employed to model process parameter effects and identify combinations that minimize surface roughness[9] .

Nevertheless, profile roughness (R_a) does not fully describe three-dimensional surface topography. Atomic Force Microscopy (AFM) provides high-resolution topographical information through areal parameters, such as S_a and S_q[10]. Among these, average areal roughness (S_a) is particularly critical for evaluating coating adhesivity, as it quantifies the true effective interfacial contact area, mechanical interlocking potential, and surface energy distribution far more accurately than linear profiles. A precise determination of S_a is paramount because functional coatings on SS316L orthopedic implants frequently undergo premature mechanical failure and delamination under in vivo physiological stress. When these coating layers break down, the bare alloy substrate is directly exposed to corrosive body fluids. Consequently, performing electrochemical corrosion measurements of SS316L in Simulated Body Fluid (SBF) is necessary to determine the alloy's passive film stability, degradation kinetics, and long-

term biocompatibility once coating integrity is compromised [11]. Furthermore, Melia et al. [12] demonstrated that surface roughness in additively manufactured SS316L is associated with localized corrosion susceptibility and breakdown potential. These findings indicate that surface evaluation should consider topographical characteristics and electrochemical responses in addition to roughness measurements.

The research gap lies in the need for an integrated evaluation connecting RSM-based optimization of SS316L turning parameters, experimental R_a validation of the produced models, AFM-based topographical characterization, and electrochemical testing in Simulated Body Fluid (SBF) using specimens produced under optimum machining conditions. Previous studies [6,7,9] primarily addressed machining characteristics and optimization, whereas studies [10,12] provide a basis for surface characterization and corrosion evaluation. Integrating these aspects may provide a more comprehensive assessment of conventionally turned SS316L surfaces.

This study optimizes the spindle speed, feed rate, and depth of cut during SS316L turning process to minimize surface roughness (R_a) using a 17-run Box–Behnken Design (BBD) Response Surface Methodology. The numerically optimized conditions were experimentally validated through repeated R_a measurements at multiple surface locations. Subsequently, the optimized specimens were evaluated via Atomic Force Microscopy (AFM) for 3D topographical parameters (S_a and S_q) and potentiodynamic polarization in Simulated Body Fluid (SBF). This framework directly links machining parameter optimization to 3D surface topography and the corrosion behavior of SS316L.

2. Materials and Methods

2.1. Materials and Machining

AISI SS316L round bars (SeAH Besteel, South Korea) with initial diameter of 16 mm and a machining length of 35 mm were used as workpieces. Turning experiments were performed using Ciamix XTRA 420 CNC lathe (Ciamix, China) equipped with DNMG 150404MS TiCN-coated carbide insert with 0.4 mm nose radius cutting tools (Kyocera, Japan). The insert was mounted on a MDJNR 2020K15 tool holder (Haas, USA). CUTSOL SP soluble cutting oil (Jumbo, Indonesia) was used as the cutting fluid.

2.2. Experimental Design and Surface Roughness Measurement

The machining experiments were designed using response surface methodology (RSM) and a three-factor, three-level Box–Behnken design (BBD). A total of 17 experimental runs consisting of 12 non-center points and five center-point replicates were generated using Minitab 2022. Spindle speed, feed rate, and depth of cut were selected as independent variable. Arithmetic mean roughness, R_a, was determined to be the response variable. The uncoded factors level and run sequence used in this study are presented in **Table 1** and **Table 2**, respectively.

Table 1. Machining parameters and experimental levels

Factor	**Parameter**	**Coded & Uncoded Variable**		
		-1	**0**	**1**
A	Spindle speed (rpm)	1450	1650	1850
B	Feed rate (mm/rev)	0.06	0.10	0.14
C	Depth of cut (mm)	0.08	0.20	0.32

R_a was measured using a Surftest SJ-310 profilometer (Mitutoyo, Japan) with a cutoff length of 3 mm and a measurement speed of 0.8 mm/s perpendicular to the turning direction. Three measurements were taken at different locations in each run.

Table 2. Box–Behnken experimental design

Run	Spindle speed (rpm)	Feed rate (mm/rev)	Depth of cut (mm)
1	1650	0.06	0.32
2	1650	0.10	0.20
3	1450	0.06	0.20
4	1850	0.06	0.20
5	1650	0.10	0.20
6	1450	0.10	0.32
7	1650	0.06	0.08

8	1450	0.14	0.20
9	1850	0.10	0.08
10	1850	0.14	0.20
11	1850	0.10	0.32
12	1650	0.10	0.20
13	1450	0.10	0.08
14	1650	0.10	0.20
15	1650	0.14	0.08
16	1650	0.14	0.32
17	1650	0.10	0.20

2.3. Model Development and Experimental Validation

The measured R_a values were analyzed using RSM in Minitab 2022. Analysis of variance (ANOVA) was used to evaluate the statistical significance of the regression model. Model adequacy was assessed based on the coefficient of determination (R^2), adjusted and predicted coefficient of determination (R^2_{adj} and R^2_{pred}), lack-of-fit test, and residual analysis. Numerical optimization was performed to minimize R_a within the investigated parameter ranges. The selected optimum conditions were subsequently used to machine a new specimen. Three roughness measurements were obtained from this specimen, and their average was compared with the predicted value to validate the model.

2.4. AFM Surface Topography and Potentiodynamic Polarization

Atomic force microscopy (AFM) measurement was done using N8 NEUS (Bruker, USA) to characterize the surface topography of the optimally machined specimen over a scan area of 10 × 10 μm². The areal arithmetic mean height (S_a) describes the mean absolute deviation of the surface from the mean plane, whereas the areal root mean square height (S_q) represents the root mean square of the surface height deviations. These parameters were used to complement the profile-based (R_a) measurement by providing three-dimensional information about the machined surface in nanometer scale as well as identifying artifacts that formed in the machined surface due to

machining process. AFM height maps and three-dimensional surface representations were used to examine the surface morphology.

The electrochemical behavior of the machined SS316L surface was evaluated by potentiodynamic polarization using CS310 electrochemical workstation (CorrTest, P.R.China) The test was conducted in simulated body fluid (SBF) media prepared according to ISO 23317:2025 at 25 °C temperature using SS316L as WE, SCE as RE, and Pt wire as CE. The exposed specimen area was set to 1 cm^2. The potential sweep was conducted from −0.2 to +0.2 V relative to OCP at a scan rate of 10 mV/s. The resulting polarization curve was used to evaluate the corrosion potential (E_{corr}) and corrosion current density (I_{corr}). The corrosion rate was determined from the electrochemical measurement results using the relevant material parameters.

3. RESULT AND DISCUSSION

3.1. Experimental Results and RSM Model Regression

Table 3 summarizes the measured surface roughness values from the 17 experimental runs conducted to measure the surface roughness variations over three variables, namely feed rate, depth of cut, and spindle speed. The response gathered from average of three surface roughness measurements from each run ($R_{a,\ avg}$) ranged from 0.220 to 0.504 µm. Smoothest surface profile was recorded in the seventh run, corresponding to spindle speed of 1650 rpm, feed rate of 0.06 mm/rev, and depth of cut of 0.08 mm. Conversely, the tenth run produced roughest surface at 1850 rpm spindle speed, 0.14 mm/rev feed rate, and 0.20 mm depth of cut. These results demonstrate that the surface finish varied considerably across the investigated machining conditions.

Table 3. Experimental design and measured surface roughness

Run	Spindle speed (rpm)	Feed rate (mm/rev)	Depth of cut (mm)	Ra_{avg} (µm)
1	1650	0.06	0.32	0.254
2	1650	0.10	0.20	0.286
3	1450	0.06	0.20	0.235
4	1850	0.06	0.20	0.223
5	1650	0.10	0.20	0.280
6	1450	0.10	0.32	0.245
7	1650	0.06	0.08	0.220
8	1450	0.14	0.20	0.450

9	1850	0.10	0.08	0.290
10	1850	0.14	0.20	0.504
11	1850	0.10	0.32	0.311
12	1650	0.10	0.20	0.332
13	1450	0.10	0.08	0.283
14	1650	0.10	0.20	0.266
15	1650	0.14	0.08	0.409
16	1650	0.14	0.32	0.455
17	1650	0.10	0.20	0.264

Visualization of the obtained data is given by contour plot for each pair of independent variables in terms of R_a, which depicted in **Figure 1(a)-(c)**. Observation of **Figure 1(a)** qualitatively indicate that there is small to no interaction between spindle speed and feed rate variables in term of R_a, and the change in R_a is mainly driven by the change of feed rate. The same deduction could also be used for **Figure 1(c)**, in which the depth of cut variable does not strongly affect the variations of R_a caused by the change in feed rate. **Figure 1(b)** gives a different picture as depth of cut is strongly interacting with spindle speed variables to influence R_a value when feed rate is held constant.

The obtained data is then fitted to a full quadratic models given by Box-Behnken Design to quantitatively evaluate each variable influences alongside the probability of significant interaction between each variable. The term yielded by the regression were tabulated in **Table 4** alongside its standard error, Student's T-value, and its significancy to the model (p-value) with CI = 0.95. The coefficient for feed rate was 0.1107, substantially larger than those for spindle speed (0.0144) and depth of cut (0.0079). Because the coefficients are expressed in coded factors, their magnitudes describe the modeled response changes relative to the coded factor scales. The variance inflation factor (VIF) was 1.00 for all three main linear factors, indicating no evidence of multicollinearity among the model terms.

Table 4. Box-Behnken Regression Parameter

Term	Coef	SE Coef	T-Value	P-Value	VIF
Constant	0.2856	0.0128	22.31	0.000	
Spindle (A)	0.0144	0.0101	1.42	0.198	1.00
Feed (B)	0.1107	0.0101	10.94	0.000	1.00
Depth (C)	0.0079	0.0101	0.78	0.462	1.00

Spindle*Spindle (A^2)	0.0076	0.0140	0.54	0.604	1.01
Feed*Feed (B^2)	0.0598	0.0140	4.29	0.004	1.01
Depth*Depth (C^2)	-0.0109	0.0140	-0.78	0.459	1.01
Spindle*Feed (AB)	0.0165	0.0143	1.15	0.287	1.00
Spindle*Depth (AC)	0.0148	0.0143	1.03	0.337	1.00
Feed*Depth (BC)	0.0030	0.0143	0.21	0.840	1.00

The resulting regression equation in coded factors is:

$$R_a = 0.2856 + 0.0144A + 0.1107B + 0.0079C + 0.0076A^2 + 0.0598B^2 - 0.0109C^2 + 0.0165AB + 0.0148AC + 0.0030BC$$

For predictions using the actual machining parameters, the corresponding equation is:

$$R_a = 1.29 - 0.00088A - 8.24B - 0.71C + 0.00A^2 + 37.39B^2 - 0.759C^2 + 0.00206AB + 0.000615AC + 0.63BC$$

where (A) denotes spindle speed in rpm, (B) denotes feed rate in mm/rev, and (C) denotes depth of cut in mm. The response is expressed in micrometers.

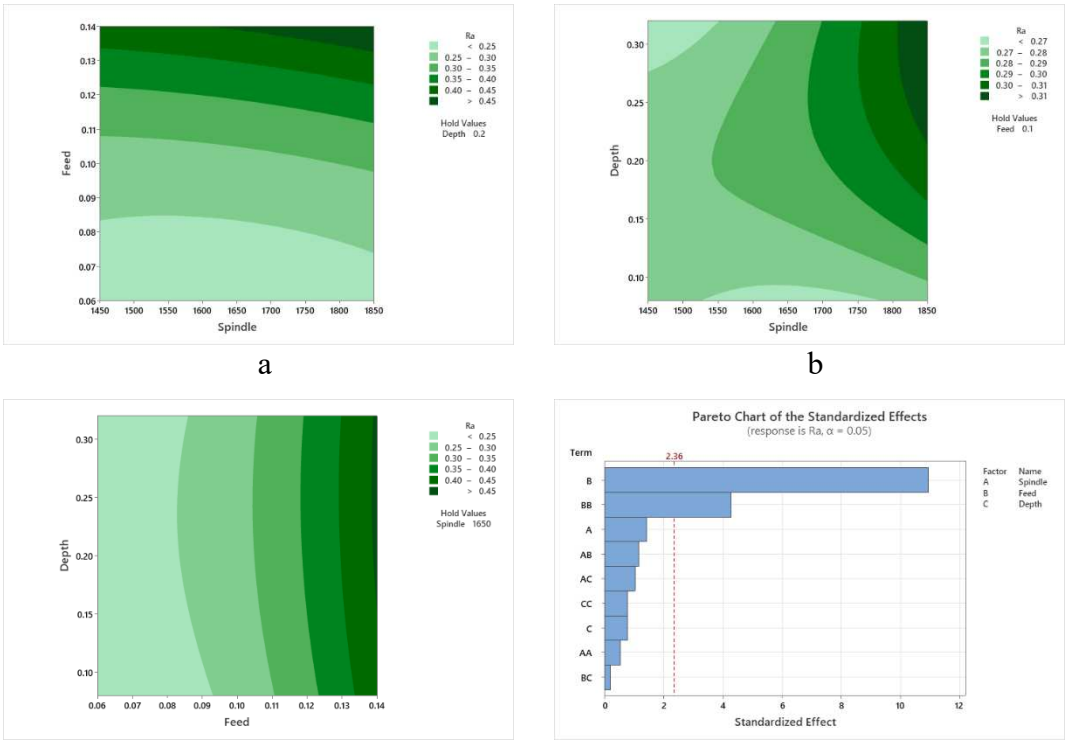
The analysis of variance (ANOVA) results for the model is presented in **Table 5**. The model had a F-value of 16.01 and a p-value of 0.001, indicating statistical significance at the 5% significance level. Evaluation of each terms reveals that out of the three linear terms (spindle speed, feed rate, and depth of cut), only feed rate lies above the significance threshold given by BBD with an F-value of 119.75 and a p-value of 0.000, which validates the observation seen in **Figure 1(a)** and **(c)**. The quadratic terms also follow the same forms as the linear terms, with only the feed rate squared terms lies above significance value (F-value 18.39, p-value 0.004). All interaction threshold lies below the significance limits.

Table 5. ANOVA results for the quadratic surface roughness model

Source	**DF**	**Adj SS**	**Adj MS**	**F-Value**	**P-Value**	**Significance**
Model	9	0.118043	0.013116	16.01	0.001	Significant
Linear	3	0.100274	0.033425	40.79	0.000	Significant
Spindle	1	0.001653	0.001653	2.02	0.198	
Feed	1	0.098124	0.098124	119.75	0.000	Significant
Depth	1	0.000496	0.000496	0.61	0.462	
Square	3	0.015774	0.005258	6.42	0.020	Significant
Spindle*Spindle	1	0.000242	0.000242	0.29	0.604	
Feed*Feed	1	0.015070	0.015070	18.39	0.004	Significant

Depth*Depth	1	0.000503	0.000503	0.61	0.459	
2-Way Interaction	3	0.001995	0.000665	0.81	0.527	
Spindle*Feed	1	0.001089	0.001089	1.33	0.287	
Spindle*Depth	1	0.000870	0.000870	1.06	0.337	
Feed*Depth	1	0.000036	0.000036	0.04	0.840	
Error	7	0.005736	0.000819			
Lack-of-Fit	3	0.002701	0.000900	1.19	0.420	Good Fit
Pure Error	4	0.003035	0.000759			
Total	16	0.123778				

The comparison of each influencing term is given in the form of pareto diagram illustrated in **Figure 1(d).** Overall, the Box-Behnken model reached 95.37% R^2, 89.41% R^2_{adj}, and 61.26% R^2_{pred}, confirming the adequacy of the model to be used in optimization study. Moreover, the Lack-of-fit parameter of the model is greater than the significance factor of 0.05, proving that the model is a good fit to the observed data.



a b

c d

Figure 1 Contour plot of **(a)** Feed rate versus Spindle Speed, **(b)** Depth of Cut versus Spindle Speed, and **(c)** Depth of Cut versus Feed rate in terms of R_a value obtained. **(d)** Standarized effect of each variable terms (linear and quadratic) alongside interaction between each variables.

Result comparison between this study and literature data reveals a variations in each variable role in influencing the workpiece surface roughness, which is summarized in **Table 6**. In all study considered in this comparison, Depth of Cut became parameter that consistently have no significant contribution to the R_a value of the machined workpiece, while spindle speed and feed rate actively influence R_a differently in different parameter regime. Low spindle speed used in this study showed no significant correlations to R_a, as also reported by Gyliene et al [13]. However, as the spindle speed increased beyond 2000 rpm as reported by Natesh et al, Kundu et al, and Avci et al [14–16], a negative correlations with R_a value began to manifest in the machining processes. These findings showed that increasing spindle speed could induce smoother machined surface in austenitic stainless steel. In this case, a decrease in R_a value is triggered by reduced friction and tool rubbing, alongside a decrease in built-up edge formations when spindle speed is increased[17]. Therefore, in the particular case where low spindle speed is necessary, either dictated by the machine capability or materials constraints, keeping it in the range of 1500-2000 rpm can provide a plateau region where spindle speed does not significantly affects the roughness of machined surface.
Comparing feed rate between each study gives more agreeable trend in relatively wide range, as all literature utilizing feed rate between 0.05 mm/rev to 0.5 mm/rev reporting a positive correlation between feed rate and increase in R_a [13,15,16]. Direct Proportionality of feed rate and surface roughness implied that the cutting tool moves further per revolution. This leaves wider tool marks, higher peaks, and deeper valleys on the workpiece, which raises the arithmetic mean roughness [18,19]. However, at very low feed rate as utilized by Natesh et al, negligible effect of feed rate to machined surface roughness is observed [14] .

Table 6. Contribution of main process parameters in terms of mean R_a

Process	**Depth of Cut (Range)**	**Spindle Speed (Range)**	**Feed Rate (Range)**	**Source**

Turning	Non-significant (0.08-0.32 mm)	Non-significant (1450-1850 rpm)	Positive correlation (0.06-0.14 mm/rev)	This study
End Milling	Non-significant (0.1-0.2 mm)	Negative Correlation (3000-4000 rpm)	Positive correlation (0.25-0.31 mm/rev)	[16]
Turning	Non-significant (0.5-1.5 mm)	Non-significant (1600-2650 rpm)	Positive correlation (0.05-0.15 mm/rev)	[13]
Turning	Non-significant (0.1-0.3 mm)	Negative correlation (1000-3000 rpm)	Positive correlation (0.2-0.5 mm/rev)	[15]
End Milling	Non-significant (1-2 mm)	Negative Correlation (2000-6000 rpm)	Non-significant (0.04-0.075 mm/rev)	[14]

3.2. Numerical Optimization

Numerical optimization of machining parameters was started by reducing the model to only its significant terms, which is the linear and quadratic feed rate terms. The reduced model gives R^2 value of 91.44%, R^2_{adj} value of 90.22%, and R^2_{pred} value of 87.00%. While the R^2 value is lower than the complete model, the R^2_{adj} and R^2_{pred} value is higher compared to the complete model, proving that the reduced model is sufficient in predicting the whole system behavior. ANOVA analysis is then repeated with only the selected terms considered to validate the reduced Box-Behnken parameters, with results tabulated in **Table 7.**

Table 7. ANOVA Result for the selected Box-Behnken terms

Source	DF	Adj SS	Adj MS	F-Value	P-Value	Significance
Model	2	0.113189	0.056594	74.82	0.000	Significant
Linear	1	0.098125	0.098125	129.72	0.000	Significant
Feed	1	0.098125	0.098125	129.72	0.000	Significant
Square	1	0.015064	0.015064	19.91	0.001	Significant
Feed*Feed	1	0.015064	0.015064	19.91	0.001	Significant
Error	14	0.010590	0.000756			
Lack-of-Fit	10	0.007555	0.000755	1.00	0.550	Good Fit
Pure Error	4	0.003035	0.000759			
Total	16	0.123778				

As the ANOVA test as well as the Lack-of Fit parameter succeeded to prove the significance of the reduced model, therefore a reduced regression equation can be used in the optimization process and is given as follows.

$$R_a = 0.3800 - 4.69\,Feed + 37.27\,Feed * Feed$$

With Feed in mm/rev.

The resulting minimization predicted by the model is then tabulated in **Table 8**. The spindle speed and depth of cut is held at its lowest value.

Table 8. Numerical optimization results

Parameter	Optimized value
Spindle speed	1450 rpm
Feed rate	0.063 mm/rev
Depth of cut	0.08 mm
Predicted R_a (Confidence Interval)	0.2327±0.0262 µm
Desirability	0.955

The predicted response range of 0.2327±0.0262 µm was used as the response range for the optimization criteria. The resulting regression curve is given in **Figure 2.**

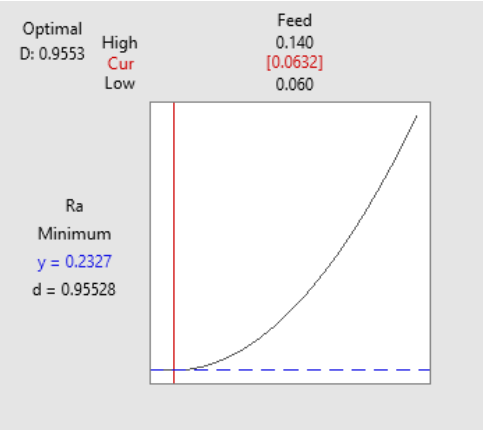


Figure 2. Numerical optimization results for minimizing surface roughness.

The selected solution is consistent with the positive feed-rate coefficient in the regression model. Since feed rate was the only statistically significant factor in the ANOVA, the optimizer selected the lower bound to minimize the predicted roughness. Consequently, the optimized combination should be understood as the minimum predicted by the fitted model under the specified constraints, rather than as proof that these settings are universally optimal for SS316L turning.

The optimized parameters were used for subsequent experimental validation and surface characterization. The validation results are particularly important because the practical usefulness of an RSM solution depends not only on the desirability value but also on its agreement with measurements obtained under the selected conditions.

3.3. Experimental Validation of the Optimum Condition

Experimental validation was conducted by machining a new SS316L specimen at the optimized settings: 1450 rpm spindle speed, 0.063 mm/rev feed rate, and 0.08 mm depth of cut. Three surface roughness measurements were obtained from the specimen. The measured values were 0.269, 0.216, and 0.247 µm, giving an average R_a of 0.244 µm.

The measured average roughness of 0.244 µm was slightly higher than the model prediction mean of 0.2327 µm, yielding an absolute difference of 0.011 µm. When the prediction error is calculated relative to the predicted value, the percentage error is approximately 4.7%. This difference indicates that the model has reached a satisfactory solution, closely relating the achievable surface finish with predicted value.

The discrepancy between real result and predicted result can be associated with experimental variability or process characteristics not explicitly represented in the regression model, such as tool condition, machine stability, coolant delivery, and local variations in roughness measurement. These factors are potential sources of variation rather than confirmed causes, as they were not independently quantified in this study.

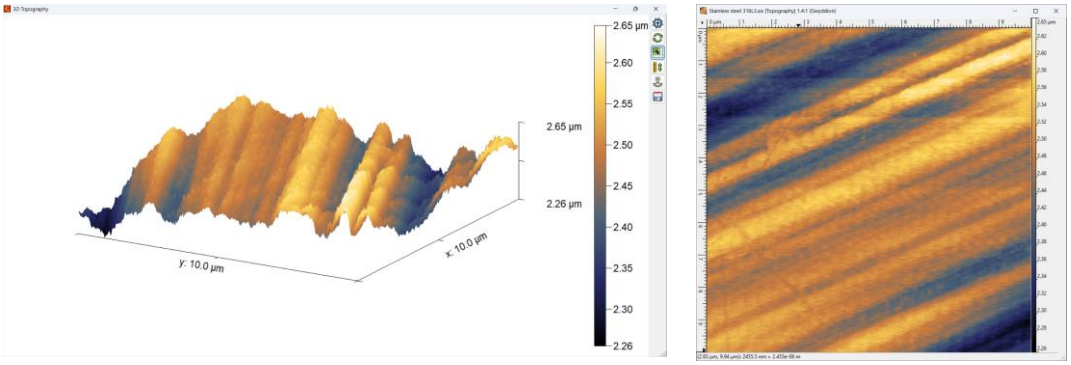
3.4. AFM Surface Topography Characterization

Atomic force microscopy with 10 × 10 μm² scan area was used to characterize the micro-scale topography of the specimen machined under the optimized condition. The areal arithmetic mean height (S_a) and root mean square height (S_q) were used to quantify surface-height variations. The areal skewness (S_{sk}) was used to describe the asymmetry of the height distribution, while the maximum surface height parameter (S_z) was used to describe the vertical extent of the surface topography. 2D and 3D AFM topography maps of the optimized specimen at the three locations are shown in **Figure 3**. Stable turning track characterized by distinct, parallel macro-ridges aligned along the processing direction surface seen in **Figure 3(a)** is diagnosed as an AFM instrument tracking artifacts caused by high-speed Z-axis controller loop oscillation as the tip slides laterally along the vertical walls of the turning groove.

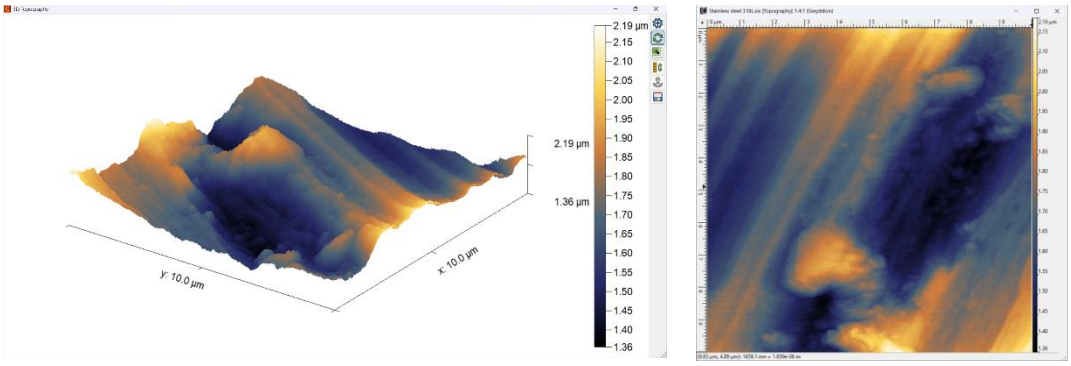
Figure 3(b) reveals a chaotic, highly disrupted surface topography caused by severe built-up edge (BUE) formation and material tearing. The map exhibits an elevated Z-axis variance stretching from 1.36 μm to 2.19 μm, defined by irregular, jagged material clusters and sharp nanoscale pits where portions of the workpiece were plucked out. This degradation occurs because the highly adhesive, ductile stainless steel periodically cold-welds itself to the TiCN-coated tool under localized cutting pressures, subsequently tearing away and dropping hardened, fragmented metal scales onto the finished surface.

Figure 3(c) illustrates a stable micro-grooving mechanism characterized by a broad, smooth trench and a rounded material ridge sweeping across the 10 μm scanning window. The surface inside this track appears ironed out and uniform, lacking the jagged tearing of the BUE phase, which indicates a phase of clean plastic deformation and side-flow. This morphology serves as a textbook geometric replication of the TiCN

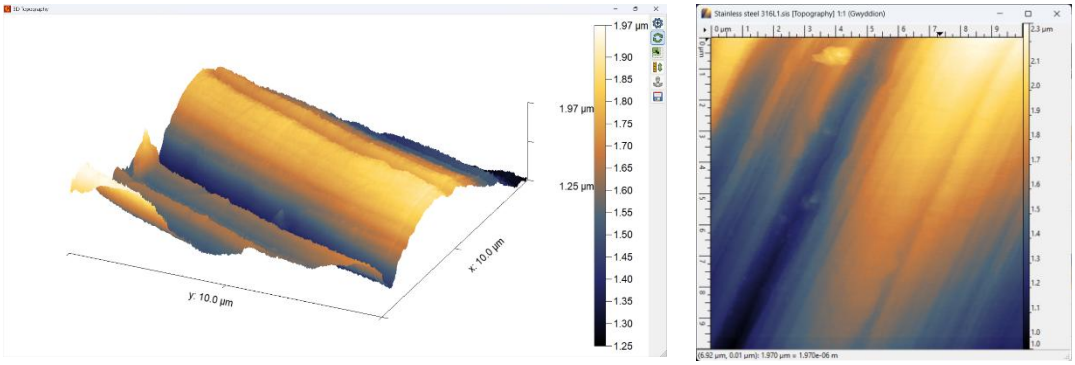
tool's nose radius smoothly plowing through the material, demonstrating the ideal surface integrity achievable when the turning parameters remain stable and free of adhesive built-up edges.



(a)



(b)



(c)

Figure 3. 2D and 3D AFM topography maps of the optimized SS316L specimen showing: **(a)** Clean machined area, **(b)** Built-up edge **(c)** Micro-grooves

Roughness parameters calculated from AFM data are summarized in **Table 9**. The S_a values were 42.11, 114.5, and 121.4 nm for locations a, b, and c, respectively. The corresponding S_q values were 55.71, 141.6, and 146.7 nm. Both parameters were substantially higher in location b and c compared to location a, indicating substantial local variation in surface-height amplitudes across the examined areas caused by the recorded built-up edge and micro-groove seen in location b and c.

Table 9. AFM surface topography parameters at the three measurement locations

Parameter	Location a	Location b	Location c
S_a (nm)	42.11	114.5	121.4
S_q (nm)	55.71	141.6	146.7
S_{sk}	-0.6977	0.1645	-0.2583
S_z (nm)	390	838	722

The negative areal skewness values at locations a and c indicate height distributions with a tendency toward a more pronounced lower-height tail, whereas the slightly positive value at location b validates the presence of built-up edge bumps.

The AFM measurements complement the profile-based roughness measurement, which yielded an average R_a of 0.244 μm (244 nm) for the validation specimen. The AFM parameters describe the topography within much smaller, localized scan areas and are therefore not directly interchangeable with the profilometer-derived R_a. The differences among the three AFM locations indicate that a single scan may not fully represent the surface topography of the entire machined specimen. These findings support the use of both profile-based and areal measurements when evaluating the surface characteristics of machined SS316L.

3.6. Potentiodynamic Polarization in Simulated Body Fluid

Potentiodynamic polarization testing was conducted to assess the electrochemical response of the optimized SS316L specimen in simulated body fluid (SBF). The result of the potentiodynamic polarization curve of the optimized specimen in SBF is shown in **Figure 4**.

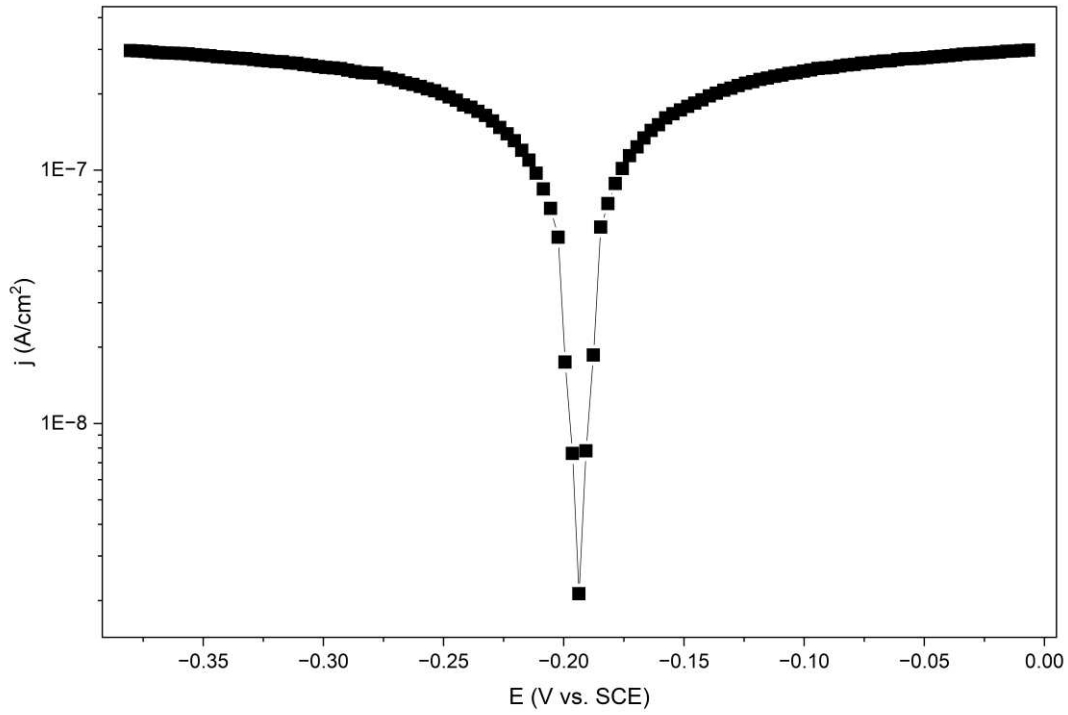


Figure 4. Potentiodynamic polarization curve of the optimized SS316L specimen in SBF.

The electrochemical parameters obtained from the Tafel extrapolation are summarized in **Table 10**. The fitted corrosion potential (E_{corr}) was −0.192 V, and the corrosion current density (I_{corr}) was 6.2847×10^{-9} A/cm² that corresponds to a corrosion rate of 6.54×10^{-5} mm/year. The anodic and cathodic Tafel slopes were found to be 141.57 and 206.61 mV/dec, respectively.

Table 10. Electrochemical parameters obtained from potentiodynamic polarization

Parameter	**Value**
Corrosion potential, (E_{corr})(V)	−0.192
Corrosion current density, (I_{corr}) (A/cm²)	6.2847×10^{-9}
Corrosion rate (mm/year)	6.54×10^{-5}
Anodic Tafel slope, (Ba) (mV/dec)	141.57
Cathodic Tafel slope, (Bc) (mVdec)	206.61

The fitted (E_{corr}) value was also more negative than the recorded OCP. Because these quantities represent different electrochemical measurements or estimates, this difference should be checked against the exported polarization curve, reference-electrode configuration, and fitting settings. The reported corrosion rate can be presented as the value obtained from the current analysis, but it should not be used alone to claim suitability for orthopedic implantation without appropriate validation and comparison.

The electrochemical results complement the surface roughness and AFM measurements by characterizing the response of the machined surface in SBF. The profilometer measurements describe the average profile roughness, while AFM provides localized information about surface-height distributions and amplitudes. Potentiodynamic polarization, in turn, evaluates the electrochemical response of the surface under the specified test conditions. Taken together, these methods provide complementary information on the surface characteristics and corrosion behavior of the optimized SS316L specimen. Nevertheless, the present results do not establish a causal relationship between individual AFM parameters and corrosion performance, because only one optimized machining condition was evaluated electrochemically.

Conclusions

RSM modelling found that between feed rate, depth of cut, and spindle speed, only feed rate significantly influences the surface roughness of SS316L workpiece. A reduced regression formula in term of only feed rate is then calculated with a R^2_{pred} value of of 87.00%. A minimization of surface roughness is then performed using the reduced model, which predicts R_a of 0.2327 μm using 0.063 mm/rev feed rate while spindle speed and depth of cut is held at 1450 rpm and 0.08 mm, respectively. Actual R_a value obtained turns out to be 0.244 μm, missing by 4.7% from the predicted value. Atomic force microscopy (AFM) revealed local variations in surface topography across the three examined locations, with built-up edge and micro-groove found in the machined surface. Potentiodynamic polarization testing in simulated body fluid (SBF) electrolyte yielded a corrosion potential (E_{corr}) of −0.192 V and a corrosion current

density (I_{corr}) of 6.2847×10^{-9} A/cm², corresponding to corrosion rate of 6.54×10^{-5} mm/year. Overall, integrating RSM-based optimization, experimental roughness validation, AFM topography characterization, and electrochemical testing provides a combined approach for evaluating the surface characteristics of machined SS316L. The identified machining condition may serve as a starting point for further process development where surface finish and electrochemical performance are important. Future work should improve predictive accuracy through additional validation experiments and examine the effects of tool wear, surface characteristics, and different exposure conditions on corrosion behavior.

CReDiT authorship contribution statement

References

[1] M. Geetha, A.K. Singh, R. Asokamani, A.K. Gogia, Ti based biomaterials, the ultimate choice for orthopaedic implants – A review, Prog. Mater. Sci. 54 (2009) 397–425. https://doi.org/10.1016/j.pmatsci.2008.06.004.

[2] B. Jillek, P. Szabó, J. Kopniczky, O. Krafcsik, I. Szabó, B. Patczai, K. Turzó, Characterizing Surface Morphological and Chemical Properties of Commonly Used Orthopedic Implant Materials and Determining Their Clinical Significance, Polymers (Basel). 16 (2024) 1193. https://doi.org/10.3390/polym16091193.

[3] M.A. Irfa'i, Yunus, R.B. Taqriban, W.D. Lestari, I.M. Arsana, Larasanto, A.R. Prayitno, Z. Ardiansyah, P. Puspitasari, A.P. Bayuseno, Synergistic effects of substrate topography and phase-transformation-induced porosity in low-cost un-stabilized zirconia bond coats for flame-sprayed hydroxyapatite coatings, Int. J. Adhes. Adhes. 153 (2027) 104490. https://doi.org/10.1016/J.IJADHADH.2026.104490.

[4] J. Botterill, H. Khatkar, The role of hydroxyapatite coating in joint replacement surgery – Key considerations, J. Clin. Orthop. Trauma 29 (2022) 101874. https://doi.org/10.1016/J.JCOT.2022.101874.

[5] J.B. Mistry, M. Chughtai, R.K. Elmallah, A. Diedrich, S. Le, M. Thomas, M.A. Mont, Trunnionosis in total hip arthroplasty: a review, Journal of Orthopaedics and Traumatology 17 (2016) 1–6. https://doi.org/10.1007/s10195-016-0391-1.

[6] K. Szwajka, J. Zielińska-Szwajka, T. Trzepieciński, Improving the Surface Integrity of 316L Steel in the Context of Bioimplant Applications, Materials 16 (2023) 3460. https://doi.org/10.3390/ma16093460.

[7] M.U. Farooq, S. Anwar, R. Ullah, R.H. Guerra, Sustainable machining of additive manufactured SS-316L underpinning low carbon manufacturing goal, Journal of Materials Research and Technology 24 (2023) 2299–2318. https://doi.org/10.1016/j.jmrt.2023.03.122.

[8] R. del Risco-Alfonso, R. Pérez-Rodríguez, P. del C. Zambrano Robledo, M. Rivas Santana, R. Quiza, Optimization of the Cutting Regime in the Turning of the AISI 316L Steel for Biomedical Purposes Based on the Initial Progression of Tool Wear, Metals (Basel). 11 (2021) 1698. https://doi.org/10.3390/met11111698.

[9] M.S. Surya, Optimization of machining parameters while turning AISI316 stainless steel using response surface methodology, Sci. Rep. 14 (2024) 30083. https://doi.org/10.1038/s41598-024-78657-z.

[10] K. Gulati, T. Adachi, Profiling to Probing: Atomic force microscopy to characterize nano-engineered implants, Acta Biomater. 170 (2023) 15–38. https://doi.org/10.1016/j.actbio.2023.08.006.

[11] A. Woźniak, M. Staszuk, Ł. Reimann, O. Bialas, Z. Brytan, S. Voinarovych, O. Kyslytsia, S. Kaliuzhnyi, M. Basiaga, M. Admiak, The influence of plasma-sprayed coatings on surface properties and corrosion resistance of 316L stainless steel for possible implant application, Archives of Civil and Mechanical Engineering 21 (2021) 148. https://doi.org/10.1007/s43452-021-00297-1.

[12] M.A. Melia, J.G. Duran, J.R. Koepke, D.J. Saiz, B.H. Jared, E.J. Schindelholz, How build angle and post-processing impact roughness and corrosion of additively manufactured 316L stainless steel, Npj Mater. Degrad. 4 (2020) 21. https://doi.org/10.1038/s41529-020-00126-5.

[13] V. Gyliene, A. Brasas, A. Ciuplys, J. Jablonskyte, Optimization of the Surface Roughness and Chip Compression Ratio of Duplex Stainless Steel in a Wet Turning Process Using the Taguchi Method, Machines 2024, Vol. 12, Page 437 12 (2024) 437. https://doi.org/10.3390/MACHINES12070437.

[14] C.P. Natesh, N.G. Siddeshkumar, G. Srinivasa, A. Shivaramakrishna, H.M. Pruthvi, C.D. Prasad, Y.M. Shashidhara, H.J. Amarendra, A. Tiwari, A.A. Aden, Multi-objective optimization of surface roughness and MRR in AISI 316L stainless steel processed by MQL end milling using taguchi, RSM, ANN,

and RFR methods, Scientific Reports 2025 15:1 15 (2025) 36583-. https://doi.org/10.1038/s41598-025-20454-3.

[15] S. Kundu, B. Choudhuri, R. Sen, CNC Machinability study of AISI 316L & Optimization of Machining parameters using TLBO algorithm, Mater. Today Proc. 62 (2022) 1218–1225. https://doi.org/10.1016/J.MATPR.2022.04.473.

[16] B. Avcı, S.O. Yılmaz, İ.S. Dalmış, Experimental Optimization of Surface Roughness In Milling of AISI 304 Stainless Steel on A CNC Vertical Machining Center, Trakya Üniversitesi Mühendislik Bilimleri Dergisi 25 (2024) 117–128. https://doi.org/10.59314/tujes.1597200.

[17] N.S. Kumar, A. Shetty, A. Shetty, K. Ananth, H. Shetty, Effect of spindle speed and feed rate on surface roughness of carbon steels in CNC turning, Procedia Eng. 38 (2012) 691–697. https://doi.org/10.1016/J.PROENG.2012.06.087.

[18] P.Y.M.W. Ndaruhadi, S. Sharif, D. Kurniawan, Effect of Different Cutting Speed and Feed Rate on Surface Roughness in Femur Bone Drilling, Procedia Manuf. 2 (2015) 208–211. https://doi.org/10.1016/J.PROMFG.2015.07.036.

[19] M.H.M. Ghazali, A.Z.A. Mazlan, L.M. Wei, C.T. Tying, T.S. Sze, N.I.M. Jamil, Effect of Machining Parameters on the Surface Roughness for Different Type of Materials, IOP Conf. Ser. Mater. Sci. Eng. 530 (2019) 012008. https://doi.org/10.1088/1757-899X/530/1/012008.